The Thesis committee for Rebecca Gabrielle Tippens

Certifies that this is the approved version of the following thesis:

Investigating planar distributions of satellites

around Local Group analogs

SUPERVISING COMMITTEE:

Michael Boylan-Kolchin, Supervisor

Volker Bromm

Investigating planar distributions of satellites around Local Group analogs

by

Rebecca Gabrielle Tippens

Thesis

Presented to the Faculty of the Graduate School

of The University of Texas at Austin

in Partial Fulfillment

of the Requirements

for the Degree of

Master of Arts

The University of Texas at Austin

December 2019

Acknowledgments

The author wishes, first and foremost, to thank supervisor Michael Boylan-Kolchin and committee members Miloš Milosavljević, Volker Bromm and Caitlin Casey for their thoughtful guidance over the course of this work.

Second, to express profound gratitude to the friends, family, and peers who acted as caregivers and advocates in times of fragile health – consistently demonstrating the healing power of simple human connection. To quote the late Michelle McNamara: "It's chaos. Be kind."

This thesis is based upon work supported by NASA grant NNX17AG29G (PI: Boylan-Kolchin).

Rebecca Gabrielle Tippens

The University of Texas at Austin

December 2019

Investigating planar distributions of satellites around Local Group analogs

by

Rebecca Gabrielle Tippens, M.A.
The University of Texas at Austin, 2019
SUPERVISOR: Michael Boylan-Kolchin

Among the various outstanding small scale challenges to ΛCDM Cosmology is the observation of apparently thin, kinematically coherent planes of satellites around galaxies in the Local Group and beyond. The issue remains remarkably contentious, with conflicting claims about the significance of observed planes, the efficacy of dark matter only simulations in exploring this phenomenon, and broad theoretical disagreement about the occurrence of planes of satellites even between analyses of the same suites of simulations. In this paper, we build upon existing analyses planes of satellites around $z = 0$ Local Group analogs in the ELVIS suite of dissipationless simulations by making use of the full ELVIS merger trees. These allow us to track the kinematic coherence and evolution of "present-day" planes back through cosmic time, and weigh in on their relation to host galaxy properties and environment. Modeling our plane search on observational claims about M31, we find that comparable distributions of $z = 0$ satellites are rare in the ELVIS simulations, but they do exist. However, their co-rotation ratios are less impressive than, for example, the apparently strong co-rotation of M31's plane of satellites, and their other properties do not hold up under further scrutiny. These planes are rarely uniquely-defined or kinematically coherent by more robust measures at $z = 0$, and

their properties vary significantly across cosmic time, even with our most generous selection criteria. We interpret these results with the aid of $z = 0$ analogs from the FIRE Latte simulations – both with and without the contribution of a stellar disk component. The Latte sample suggests that a stellar disk potential helps create less radially concentrated, more statistically significant present-day planes but, as with our ELVIS DMO sample, these configurations are not particularly kinematically coherent by our metrics. We therefore conclude that, to the degree that planes like M31's exist in the ELVIS simulations, they are chance alignments of satellites that do not constitute a significant challenge to CDM. Finally, we weigh in on existing arguments concerning the utility of DMO simulations in plane analyses, demonstrating that thoughtful subhalo sample selection can help systems from DMO simulations recreate the kinematic effects of a baryonic contribution in the form of a stellar disk potential.

Contents

Chapter 1

Introduction

The concordance cosmological model, in which our Universe is dominated by constant dark energy (Λ) and cold dark matter (CDM), has been remarkably successful at explaining observations of large scale structure ($\gtrsim 10$ Mpc). However, challenges persist on galactic and sub-galactic scales; in particular, the observed abundance, distribution, and mass-density profiles of low-mass galaxies continue to defy model predictions (Bullock & Boylan-Kolchin, 2017). The observed spatial distribution of satellite galaxies around their hosts is perhaps the longest-running conflict in near-field cosmology, yet it is also arguably the least-studied. In CDM theory, structure forms via the hierarchical assembly of dark matter haloes, one result of which is the approximately isotropic distribution of substructure in dark-matter-only (DMO) simulations. If observed dwarf satellites correspond to some subset of this DM halo population, we would expect their spatial distribution to reflect that fact. Yet,

observational claims of flattened distributions ("planes") of satellite galaxies span nearly half a century.

The first evidence of planar structure came from Lynden-Bell (1976), who observed that the 11 brightest satellites of the Milky Way lie in a thin plane oriented nearly perpendicular to the Galactic disk. Later studies used proper motion measurements to show that many of these satellites are co-rotating, suggesting that the plane is rotationally supported (Metz et al., 2008; Pawlowski et al., 2013). A comparable structure has been observed in the dwarf satellite population of M31 (Koch & Grebel, 2006). Ibata et al. (2013) found that $\sim 50\%$ of its satellites lie within a vast, thin plane, and radial velocity measurements of these objects suggest that 13 of the 15 are co-rotating.

There are also claims of satellite planes outside of the Local Group (Chiboucas et al., 2009; Bellazzini et al., 2013), most notably around the galaxy Centaurus A (Cen A). Tully et al. (2015) described evidence for two distinct but nearly parallel planes in the Cen A Group, arguing that the system's approximately edge-on orientation left little room for ambiguity regarding satellite distribution. Müller et al. (2016) combined the Tully et al. (2015) sample with line-of-sight positions of dwarf galaxies considered to be candidate Cen A group members to argue that, despite the apparent "dip" in satellite density near the mid-plane of the system, statistical analysis favors a unimodal satellite distribution – a single plane.

One explanation for the seemingly unlikely morphologies of the aforementioned systems is that filamentary accretion of substructure onto a host galaxy can produce a flattened distribution of satellites. This mechanism is supported by a number of simulations (e.g., Libeskind et al., 2005), and used by Buck et al. (2015) to question the significance of observed planes around the MW and M31 as a challenge to CDM. Others have proposed that the satellites comprising local planar structures are, in fact, "tidal dwarf galaxies" (TDGs) – remnants of a single, significant galaxy interaction that shaped the Local Group as we know it today (e.g., Kroupa, 2012). However, this explanation appears to be in conflict with the observed mass-metallicity relation for dwarf satellite galaxies (Kirby et al., 2013).[1]

Indeed, there is ample evidence to suggest that baryonic processes alter the spatial distribution of satellite galaxies around their host. Numerous hydrodynamical simulations indicate that the presence of a central galaxy tends to lead to the tidal destruction of nearby substructure (e.g., Wetzel et al., 2016; Garrison-Kimmel et al., 2017), in some cases leaving a satellite population that is entirely separate from its DMO counterpart (e.g., D'Onghia et al., 2010). Ahmed et al. (2017) even argue that baryonic physics is critical to our understanding of the plane problem. In their simulations, statistically significant planes are *only* possible via the inclusion of baryonic processes to deplete the inner ∼20 kpc of the system and shape a distinctly

[1]For another perspective, see Recchi et al. (2015).

different, less radially-concentrated subhalo population.

Other criticisms of the "plane problem" are rooted in statistics. Buck et al. (2016) found that planes with properties comparable to that of M31 are common in their simulations – chance alignments that may appear co-rotating from a variety of viewing angles – but they are not kinematically coherent by more robust measures such as the clustering of angular momentum vectors in the plane, and not persistent in their properties when traced back in time. Cautun et al. (2015) raise similar critiques by defining a statistic (the plane "prominence") to quantify the relative likelihood of a given satellite alignment occurring by chance, and conclude that $\sim 5\%$ of galactic haloes in their simulations have alignments more prominent than that of the MW, and $\sim 9\%$ more prominent than the plane of M31. They therefore argue that accounting for the *look-elsewhere effect* reduces the claimed statistical significance of plane detections in the Local Group, such that at least local observational claims would no longer clash with CDM predictions.

Chapter 2

Planes of satellites in Local Group analogs

2.1 Scientific Justification

However compelling one finds the arguments outlined in Chapter 1, recent observations of the Cen A group have revitalized the plane debate. Müller et al. (2018) evaluated dwarf galaxy kinematics around Cen A and found a single, thin plane of satellites with a level of co-rotation found in $< 0.5\%$ of analogous systems in standard cosmological simulations; this, even with the inclusion of baryonic physics (gas physics, star formation and feedback processes) and conditional statistics to mitigate the look-elsewhere effect. The authors are gradually expanding their study to the larger Centaurus group (Cen A, M83, and their satellites), enabling greater comparison with local observations (Müller et al., 2019).

For the time being, though, the Local Group continues to provide the best and most complete dataset for analysis of small-scale challenges to the cosmological concordance model. Within it, many questions persist: Are the products of high-resolution dissipationless simulations sufficient to model satellite galaxy distributions, or do baryonic processes play a crucial role in plane formation? If so, which processes in particular? What statistics best describe the significance of one plane detection relative to another, and to simulation results?

In this work, we approach the above questions from several angles. First, we build upon existing analyses of planes of satellites around $z = 0$ Local Group analogs in the ELVIS suite of dissipationless simulations (Pawlowski et al., 2012; Pawlowski & McGaugh, 2014) by making use of the full merger trees. These allow us to track the kinematic coherence and evolution of "present-day" planes across cosmic time, and weigh in on their relation to host galaxy properties. We separately assess the spatial and kinematic properties of satellites around $z = 0$ LG analogs from the FIRE Latte simulations, with and without baryonic contributions, and compare them with the ELVIS results to weigh in on the significance of LG plane detections and the relative value of different types of simulations in assessing them.

In § 2.2, we describe the simulation suites used to generate our sample of LG analogs, and outline our routine for fitting planes of satellites and studying the spatial and kinematic evolution of their components. In § 2.4, we describe the

properties of $z = 0$ planes found in our DMO sample and, where possible, dissect those properties as a function of time. In § 2.5, we do the same for the DM+disk sample at $z = 0$. Finally, we compare our results to the existing literature in § 2.6, and discuss their implications for future studies of satellite planes and other small-scale challenges to the concordance cosmological model.

2.2 Halo Sample

2.2.1 ELVIS haloes

Exploring the Local Volume in Simulations (ELVIS) is a suite of high-resolution dissipationless simulations modeling the Local Group in a cosmological context (Garrison-Kimmel et al., 2014). The full ELVIS data release includes merger trees and $z = 0$ halo catalogs for 48 simulated Galaxy-sized haloes – 12 Local Group analog halo pairs and 24 mass-matched isolated haloes – each within a high-resolution volume of 2-5 Mpc and with surrounding substructure resolved down to a peak mass of $M_{peak} = 6 \times 10^7 M_\odot$. Notably, the authors find no significant difference in the abundance or kinematics of substructure within the virial radius of isolated hosts compared to their paired counterparts. On larger (Mpc) scales, however, the paired hosts average nearly twice as many subhaloes, and the kinematics of subhalo populations are hotter and more complex in the paired environments.

Of the Local Group-analog pairs in the ELVIS suite, Zeus & Hera provide

the most promising comparison to our own system (M31 and the MW, respectively). Garrison-Kimmel et al. (2014) note that the virial volumes of the two galaxies in this system overlap, but the effects of this feature should be negligible because only one subhalo resides in the overlapping volume.

2.2.2 FIRE Latte haloes

The Latte simulation suite is an extension of the Feedback In Realistic Environments (FIRE) project focused on ultra-high resolution simulations of MW-like galaxies (Garrison-Kimmel et al., 2017). In this work, the authors compare simulations of two separate haloes across each of three scenarios: (1) dark matter-only (DMO) (2) full baryonic physics, and (3) dark matter with the addition of a stellar disk potential matching the one from the FIRE simulation. They find that the third scenario does an excellent job of reproducing the number and spatial distribution of satellites from the full hydrodynamical simulation at a fraction of the computational cost. We thus consider only the first and third scenarios in this analysis, using the $z = 0$ results to examine the effects of a stellar disk potential on planar distributions of satellites.

2.2.3 Physical consistency in our samples

The peculiarities of different algorithms for tracking dark matter haloes and assembling their merger histories inevitably results in some number of physically incon-

sistent objects within a given simulation. The nature of this inconsistency depends in large part on the relative importance assigned to various halo properties (e.g., halo mass, position, circular velocity,) and subjective plausibility of various changes between simulation timesteps. While dynamically inconsistent objects might only slightly bias larger population studies, they can significantly impact outcomes on the scale of our work.

The halo catalogs and main branches presented in Garrison-Kimmel et al. (2014) were generated using the `ROCKSTAR` halo finder (Behroozi et al., 2013a) and `Consistent Trees` algorithm (Behroozi et al., 2013b). For the Latte haloes from Garrison-Kimmel et al. (2017), the authors used the `AMIGA` halo finder (`AHF`) (Knollmann & Knebe, 2009) and `Consistent Trees` to get to the $z = 0$ catalogs used here.

A preliminary analysis of the time evolution of M_{vir} (and, to a lesser extent, V_{max}) for ELVIS subhaloes chosen by our plane fitting routine reveals a small number of objects of questionable physical consistency. While `Consistent Trees` breaks "problematic" links in merger trees on the basis of mass, position, and velocity continuity, it does not explicitly prioritize mass consistency in repairing them. Instead, it ranks the potential progenitors by their relative proximity in position-velocity phase space and chooses the nearest (i.e., highest likelihood) within a certain threshold. It is therefore the case that unphysical changes in M_{vir} (often corresponding to major

mergers) may slip through the cracks – particularly when it comes to subhaloes, for which M_{vir} and V_{max} are not necessarily correlated.

We emphasize the importance of removing such gravitationally inconsistent objects from precision analyses like this one. Although they are decently rare, their erratic mass evolution seems to bias at least the initial steps of our fitting routine in their favor because we begin with the subset of satellites with the largest values for M_{peak}. Even when these objects are not chosen for the "best-fit" plane for a given sample, their initial inclusion inevitably invites comparison with satellites outside of observed planes (e.g., the 12 dwarf galaxies which lie beyond Andromeda's observed planar structure in Ibata et al. (2013)). We experiment with various thresholds for what is considered an unphysical change in M_{vir} between adjacent timesteps and find that the initial link-breaking threshold of 0.5 dex from Behroozi et al. (2013b) works nicely. We henceforth refine our ELVIS sample to exclude all haloes with a factor of five or greater change in virial mass between adjacent timesteps.

2.3 Plane-fitting Routine

2.3.1 Fitting at $z = 0$

Drawing on observational results from Ibata et al. (2013), we define our "best-fit" solution as the thinnest plane that can be fit using half of the 30 most massive subhaloes within the virial radius of each host. We find this solution by taking

the full catalog of subhaloes in the simulation volume of the host, eliminating all objects outside of its virial radius ($\sim$300 kpc at $z = 0$), and selecting the 30 most massive. With this sample in place, we randomly generate normal vectors from a uniform spherical distribution, each representing a plane centered on the origin, and compare the root-mean-square (RMS) distances, or thicknesses, of the 15 subhaloes closest to this "test" plane to find the thinnest. The RMS radial distance of this subhalo population, while also calculated and included in our results, is not expressly minimized or maximized by this routine. We consider 10,000 test plane orientations per host halo.

We also experiment with the plane definition from Buck et al. (2016), in which the best-fit solution minimizes the RMS thickness of the plane while maximizing the number of objects fit. For each of the 10,000 attempted planes in our fit, we test if more objects can be added to the fit without any increase in the RMS thickness to four significant figures. Where this proves possible, we use the corresponding plane as our final fit. Otherwise, the first instance of the thinnest plane is used and the number of planes of the same thickness to four significant figures is noted.

One subject of particular interest in this analysis is the relative uniqueness of each best-fit plane. The existence of numerous and diverse thin plane solutions for a given host clearly undermines any apparent planar symmetry. We examine the uniqueness of our fit results by plotting the RMS thickness of the thinnest possible

configuration of 15 subhaloes as a function of normal vector orientation.

Of course, the present configuration of subhaloes matters very little if it is not kinematically coherent. We must consider the motion of the subhaloes comprising each best-fit plane: Are they co-rotating, or will the apparent structure dissipate as the subhaloes slowly scatter? We determine the dominant motion of each host's best-fit plane by calculating the perpendicular components of its individual subhalo orbital poles and generating number counts of objects rotating in each direction. These counts allow for direct comparison with observational claims of rotationally supported (i.e., highly co-rotating) planes of satellites in the literature within a more robust analysis of the three-dimensional kinematics of each plane configuration.

For each host, we also plot the angular separation, in degrees, of individual subhalo orbital poles from their perpendicular components to demonstrate how much of the motion of each subhalo is in the plane. The goal in doing so is to provide a more nuanced understanding of each co-rotation ratio.

Finally, we employ a statistic known as the spherical standard distance (SSD) to quantify scatter in the motion of the subhaloes comprising the plane. There are multiple definitions of this quantity and approaches to its application in the literature, but we follow the convention from Buck et al. (2016). The SSD of each plane is calculated using the formula below, in which $\hat{n}_i$ represents the individual components of a satellite's angular momentum, k is the number of satellites in the

sample, and $\vec{n}$ is the mean angular momentum vector across all k satellites. We include the full sample comprising each plane in our calculations, as opposed to choosing subsets of more favorable kinematic coherence.

$$\text{ssd} = \sqrt{\frac{\sum_{i=1}^{k}[\arccos(|\langle\vec{n}\rangle \cdot \hat{n_i}|)]^2}{k}} \tag{2.1}$$

2.3.2 Fitting across cosmic time

Having performed a full kinematic analysis of the $z = 0$ results from both simulation suites, we use the ELVIS merger trees to examine the evolution of planar distributions of satellites across cosmic time. Several variations of this analysis are worthwhile, but we focus on the one which is most pertinent to local observations. We find the best-fit plane at $z = 0$ via the same routine previously described, and track the component subhaloes back in time. At subsequent timesteps, the routine first fits the n subhaloes from the $z = 0$ best-fit plane that are still within the virial radius of the host. Then, as necessary, it finds the $30 - n$ largest subhaloes within the virial radius.

Preliminary analysis of the ELVIS merger trees via this expanded routine highlights two distinct populations of satellites around each host: 1) subhaloes that are found at significant distances at earlier times but settle within the virial radius by $z = 0$, and 2) subhaloes which orbit at least partially within the virial radius at

earlier times and which lie within it at $z = 0$. Both are shown in Figure 2.1. For analysis of the ELVIS merger trees, we henceforth refine our "best-fit" definition to consider the relative impact of each population on the spatial and kinematic evolution of the planes in our study. We examine three possibilities for plane composition:

(I) In the most generous "persistent plane" scenario, a given plane of satellites is comprised entirely of subhaloes whose motions have been dominated by its gravitational influence since early times. Thus, such a plane would contain only objects from the second population described above. Visual inspection of figures such as Figure 2.1 for each host suggests the following means of minimizing the contribution of the first (infalling subhalo) population: Keep only the objects that pass within ~ 1.5 times virial radius before $z \sim 0.4$. We thus make this condition the defining property of Sample I, which will henceforth be the primary focus of this work.

(II) It is possible that the criteria used to generate Sample I could bias our results against certain observed $z = 0$ properties. Accordingly, we perform a "neutral" version of the analysis with no constraints on the infall time of the chosen satellites. Thus Sample II is the full

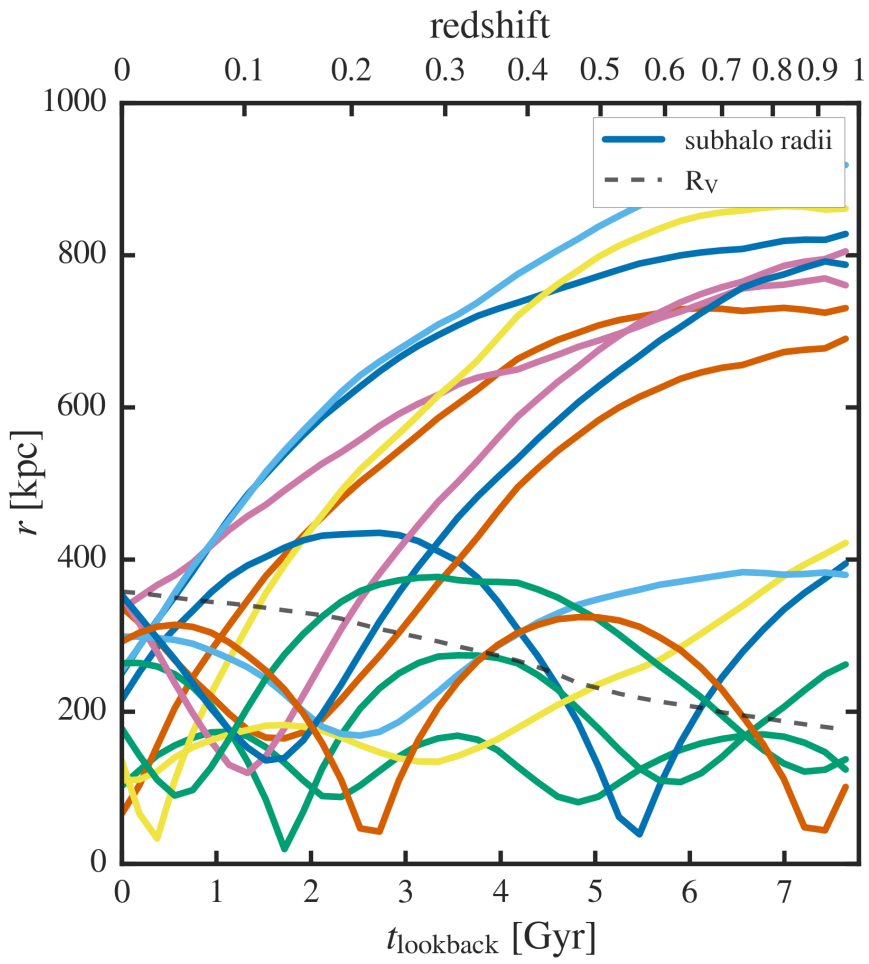

Figure 2.1: Radial distance of iZeus subhaloes from their host in preliminary ELVIS results (later referred to as "Sample II") as a function of time. This figure illustrates the bimodality observed in the spatial evolution of subhalo populations comprising $z = 0$ best-fit planes across the ELVIS sample. While the relative proportion of each population and their separation in parameter space differ somewhat between the paired and isolated host configurations, we find that we can reliably separate them with selection criteria based on the time of a subhalo's first infall.

sample of subhaloes with gravitationally consistent progenitors.

(III) Finally, we consider the inverse of our Sample I criteria for comparison with various claims from the literature regarding relevant underlying physical mechanisms.[1] Sample III is comprised primarily of objects experiencing their first infall at later times ($z \lesssim 0.4$).

2.4 DMO Results

2.4.1 ELVIS: Sample I

At $z = 0$, the RMS thickness of the thinnest plane solution averages 22.9 kpc across the 48 ELVIS hosts, with a minimum value of 13.7 kpc (for Oates in the paired configuration), and a maximum of 36.6 kpc (Lincoln in the paired configuration). The RMS radial extent of the plane is, on average, 183.4 kpc, with a minimum value of 123.5 kpc (Hera in the paired configuration) and a maximum of 230.5 kpc (iHamilton). The best-fit plane solutions for the most successful Local Group analog pair, Zeus and Hera, are shown in Figure 2.2 and Figure 2.3, respectively.

In most cases, these thin plane solutions are far from unique. Visual inspection of plots such as Figure 2.4 and Figure 2.5, showing the thickness of the

[1] These mechanisms are particularly well-summarized in Section 3.2 of Garrison-Kimmel et al. (2017), along with the choice of M_{peak} to differentiate between total subhalo destruction and mass-loss due to tidal stripping.

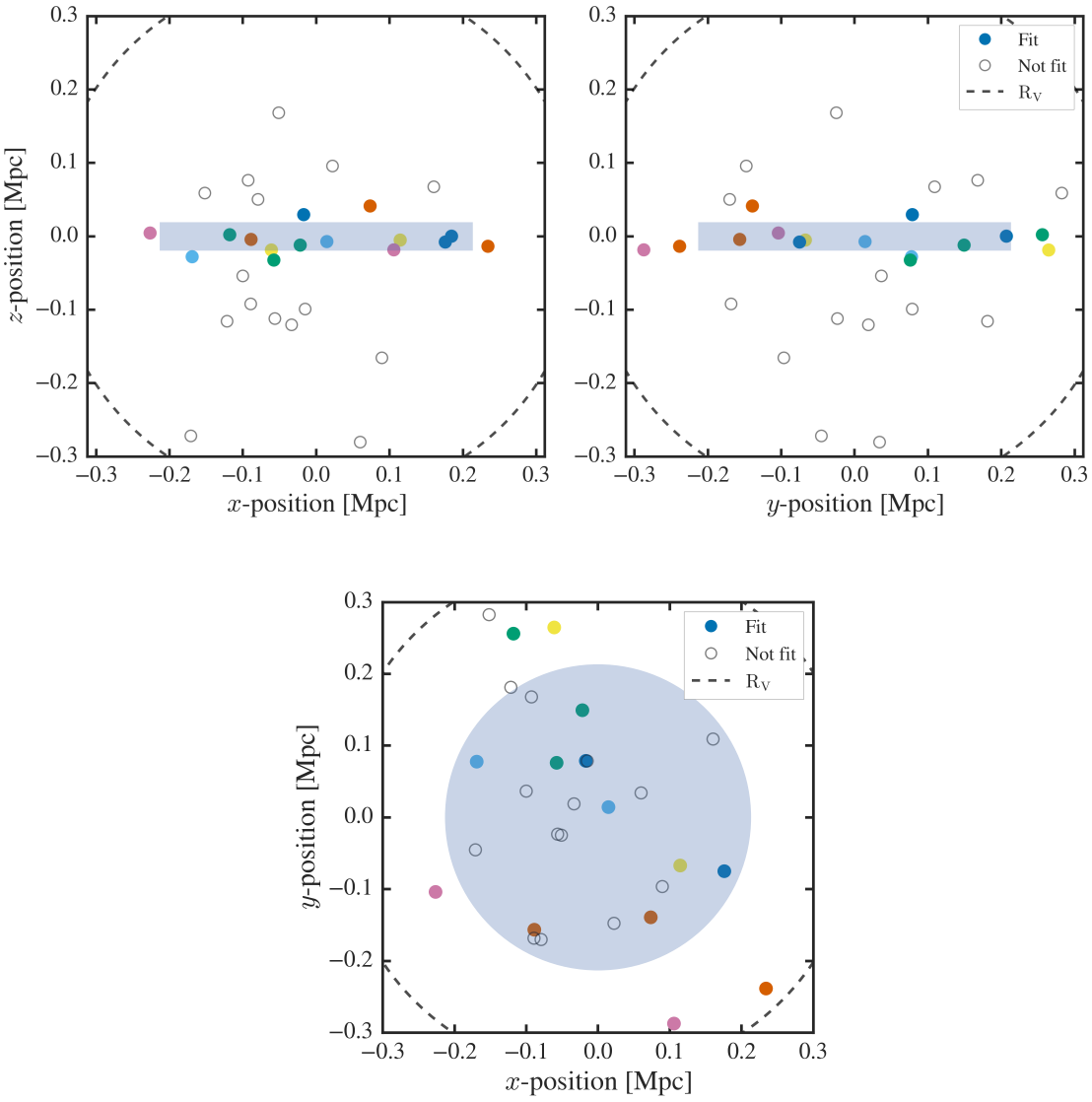

Figure 2.2: (*top*) Edge-on view and (*bottom*) face-on view of the $z = 0$ best-fit plane solution for the ELVIS Sample I paired version of Zeus (the M31-analog in the Zeus & Hera system), which has an RMS thickness of 19.2 kpc and RMS radius of 213.3 kpc.

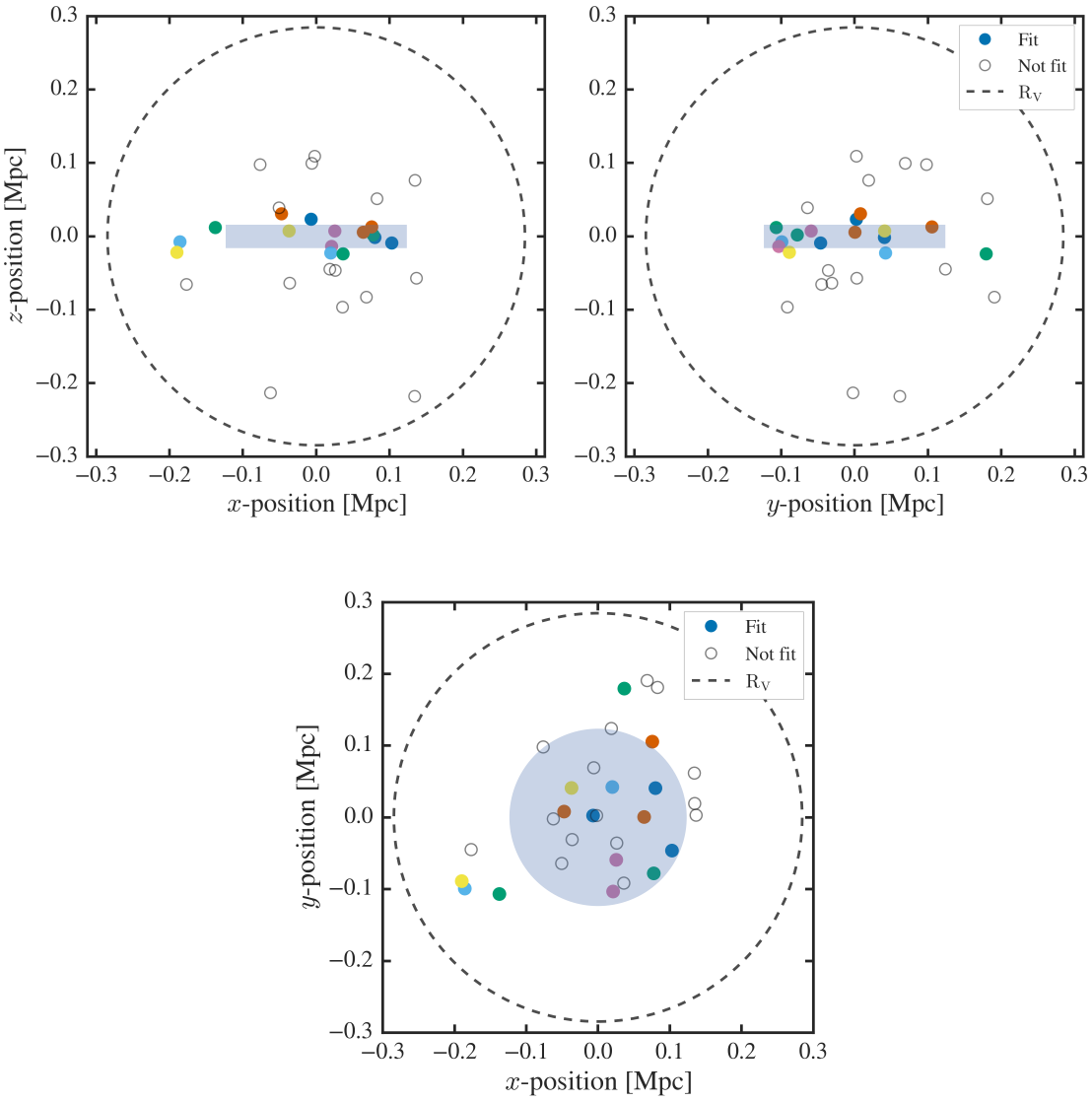

Figure 2.3: (*top*) Edge-on view and (*bottom*) face-on view of the $z = 0$ best-fit plane solution for the ELVIS Sample I paired version of Hera (the MW-analog in the Zeus & Hera system), which has an RMS thickness of 15.9 kpc and RMS radius of 123.5 kpc.

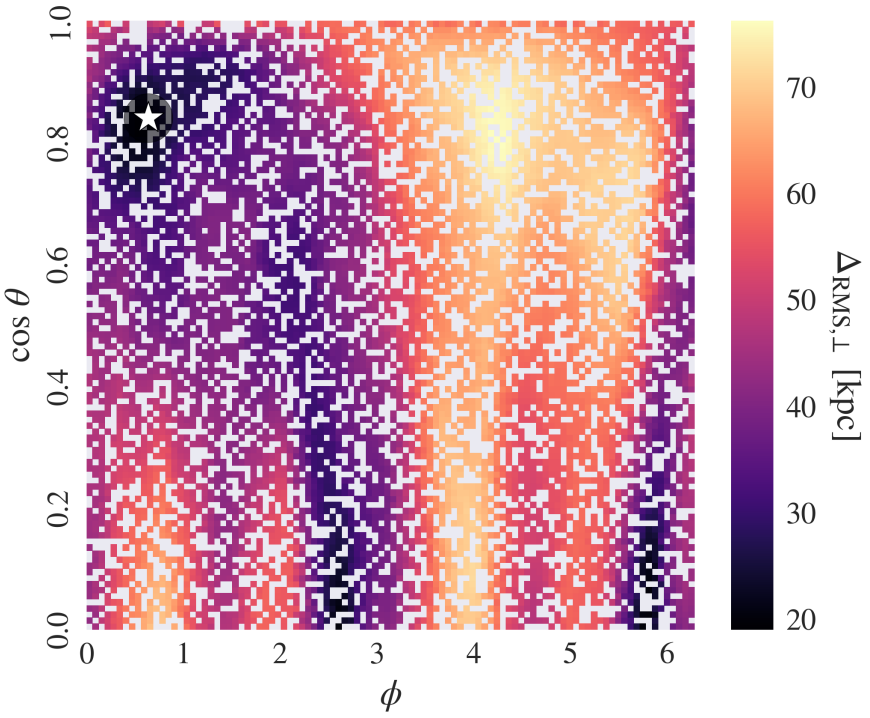

Figure 2.4: Uniqueness of the $z = 0$ best-fit plane for the ELVIS Sample I paired version of Zeus, as indicated by RMS thickness of the thinnest plane of 15 satellites as a function of test plane orientation. Each combination of values represents a normal vector with a different orientation in spherical coordinates. This plane solution is not particularly unique, and indeed no plane solution for this host exceeds an RMS thickness of $\sim$75 kpc.

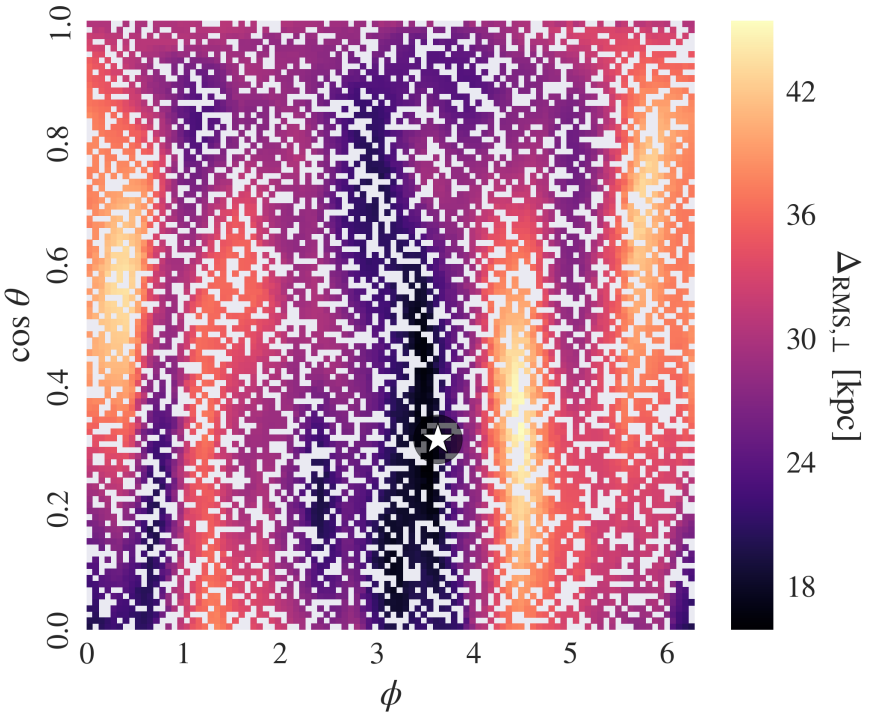

Figure 2.5: Uniqueness of the $z = 0$ best-fit plane for the ELVIS Sample I paired version of Hera. Like its partner, Zeus, this host's solution is not particularly unique. However, it is worth noting that no plane solution for this host exceeds an RMS thickness of $\sim$45 kpc.

thinnest plane of 15 satellites around a given host as a function of test plane orientation, reveals that in nearly every case a significant fraction of the parameter space is occupied by equivalent or comparable solutions. In fact, our algorithm returns planes of $\lesssim 70$ kpc at *any orientation* for $> 60\%$ of the hosts in our sample, and the thinnest plane solution never exceeds $\sim$100 kpc for any host.

The kinematics of these planes vary widely. By co-rotation ratio alone, it would appear that 12.5% of the hosts have 11 of 15 satellites co-rotating. However, when we plot the angular separation, in degrees, of individual subhalo orbital poles from their perpendicular components, we find that most of the satellite motions are primarily out of the plane for well over half of the host haloes. Furthermore, of the six most strongly co-rotating planes as judged by perpendicular component of angular momentum alone, only half have motion which is primarily within the plane – and even these show quite large scatter in their trajectories. Indeed, the lowest SSD in our sample is 33.6 degrees, and the average across all hosts 54.9 degrees.

For Sample I, the majority of the best-fit planes exhibit dramatic variations in the thickness between $z = 0$ and $z = 1$, generally hovering between $\sim$50-100 kpc and with most of their subhaloes leaving the host's virial radius before $z = 0.5$ (see Figure 2.7 and Figure 2.8. One notable exception is iOrion, which retains at least 11 of its 15 subhaloes at all times out to $z = 1$ and rarely exceeds an RMS thickness of $\sim$50 kpc. It is also worth specifying that we see little difference in the thickness

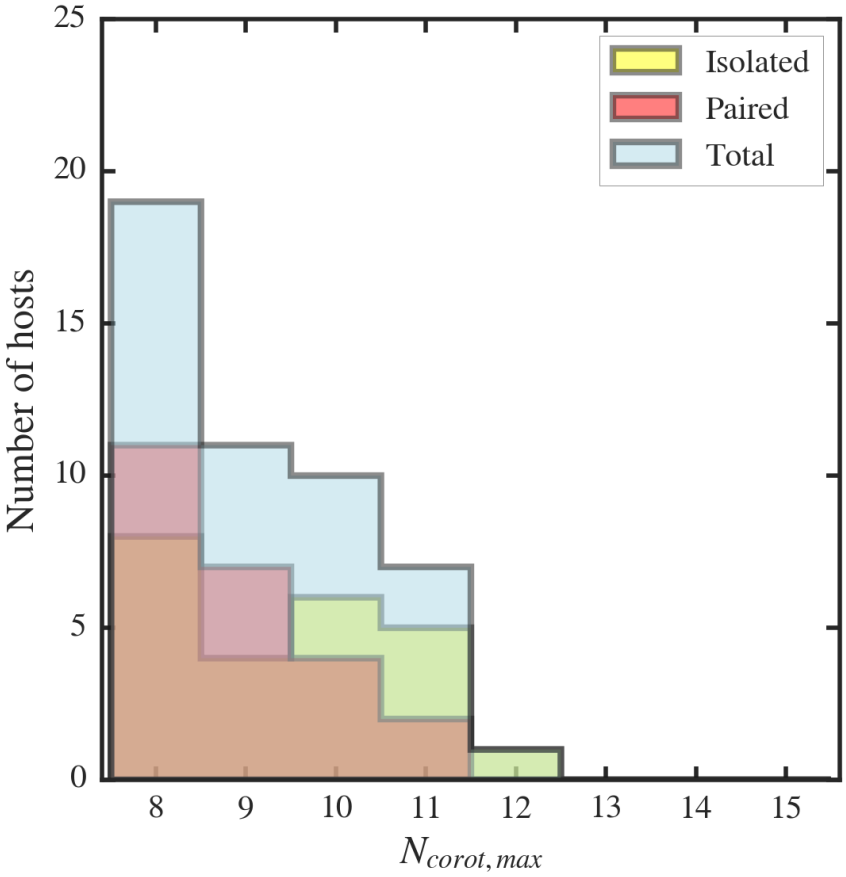

Figure 2.6: Largest number of "co-rotating" satellites in $z = 0$ planes across all 48 ELVIS Sample I hosts.

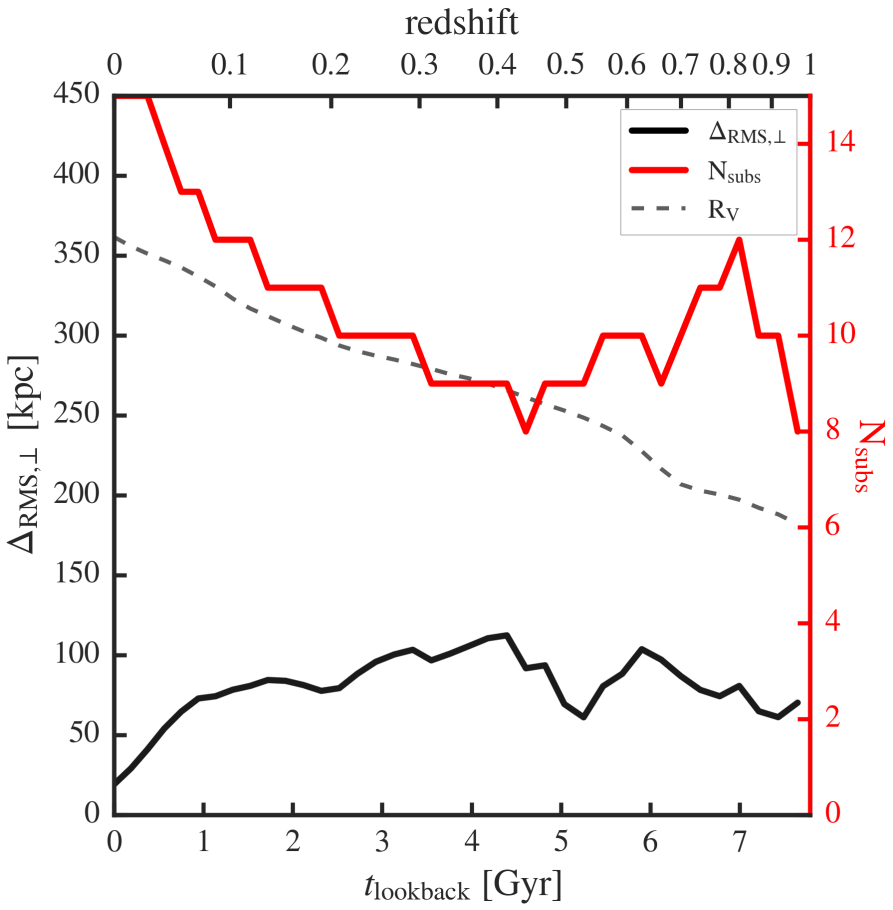

Figure 2.7: Time evolution of the thickness of the $z = 0$ best-fit plane for the ELVIS Sample I paired version of Zeus and number of component subhaloes still within its virial radius.

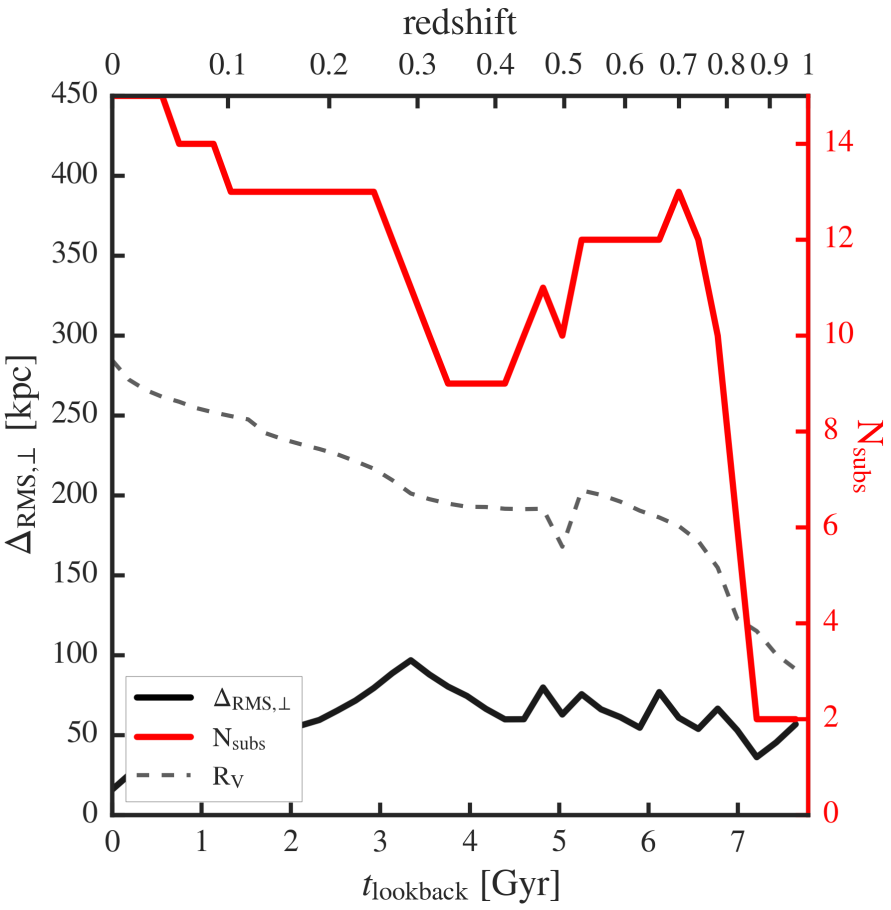

Figure 2.8: Time evolution of the thickness of the $z = 0$ best-fit plane for the ELVIS Sample I paired version of Hera and number of component subhaloes still within its virial radius.

parameter space occupied by the paired and isolated host configurations across cosmic time, a finding which appears to be consistent with results from Garrison-Kimmel et al. (2014) that *within the host's virial radius*, there is no significant difference in the spatial distribution or kinematic properties of substructure between the paired and isolated halo configurations.

As for the kinematic evolution of these planes, we find that, in most cases, the average angular momentum vector orientation of the best-fit plane repeatedly changes sign normal to the plane, meaning that the average co-rotation of the component subhaloes reverses. In fact, only 12.5% of hosts in our sample maintain their average direction of co-rotation out to $z = 1$, and these still exhibit extremely large average scatter about the mean angular momentum vector.

Finally, we probe the persistence of the planes in our sample via the initial infall times of their component subhaloes. The average redshift at which the chosen subhaloes first enter the host's virial radius ranges from $z \sim 1.57$ for pDouglas to $z \sim 0.67$ for iRemus. More context for these values is provided in Figure 2.9.

2.4.2 ELVIS: Sample II

At $z = 0$, the RMS plane dimension statistics for the full ELVIS sample (Sample II) are comparable to Sample I, albeit systematically larger by a few kpc. The RMS thickness of the thinnest plane solution averages 24.4 kpc across the 48 ELVIS hosts,

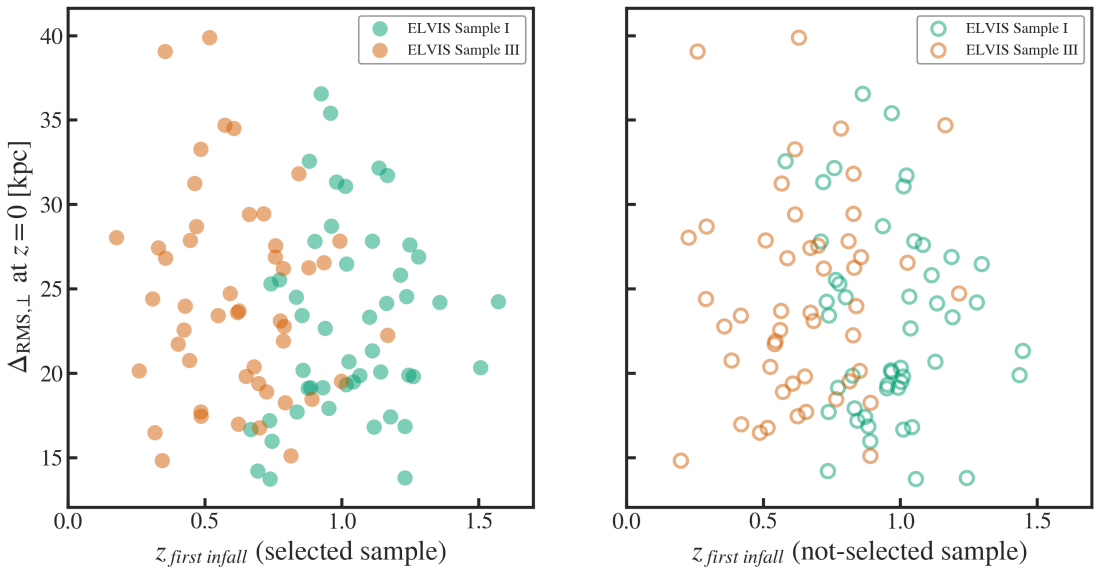

Figure 2.9: RMS plane thickness at $z = 0$ vs. average redshift of first infall for (*left*) the 15 subhaloes selected for the best-fit plane, and (*right*) the remainder of the 30 largest subhaloes that were not selected by our fitting routine (as ranked by peak virial mass, M_{peak}). These plots serve as a useful check of our Sample I selection criteria and demonstrate that even alternative subhalo selections within the Sample I plane fits would tend to produce more persistent planes with marginally smaller RMS thicknesses at $z = 0$.

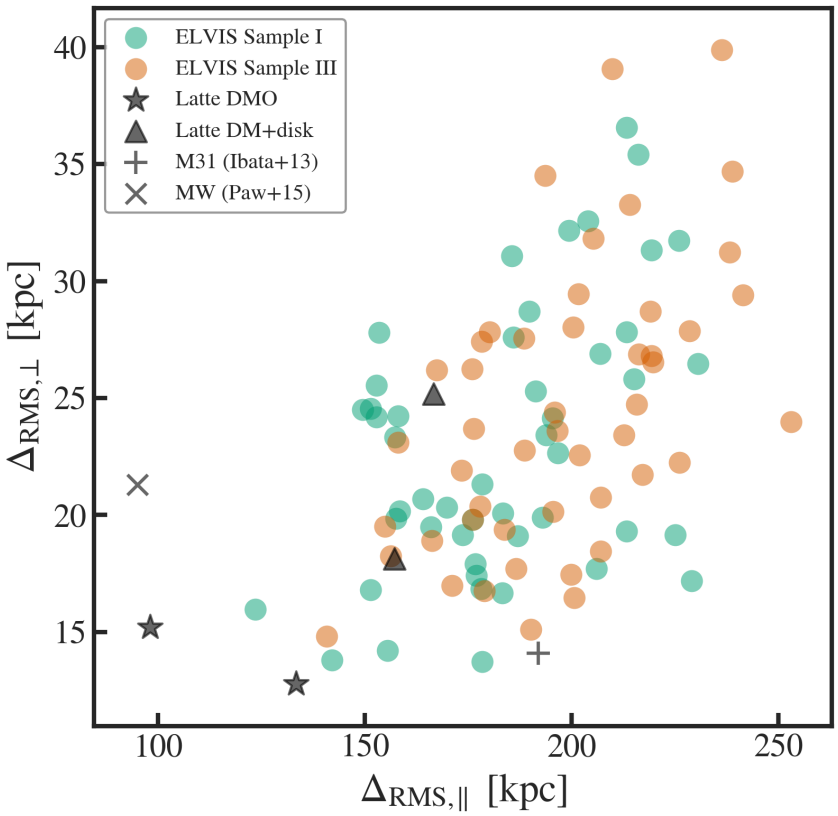

Figure 2.10: RMS thickness vs. RMS radius of the $z = 0$ best-fit plane for each host halo in this study. Observed planes for MW and M31 (from Pawlowski et al. (2015) and Ibata et al. (2013), respectively) are overplotted for comparison.

with a minimum value of 14.8 kpc and a maximum of 39.8 kpc. The RMS radial extent of the plane is, on average, 197.2 kpc, with a minimum value of 140.8 kpc and a maximum of 242.7 kpc.

By co-rotation ratio alone, the kinematics of the planes in this sample appear slightly more coherent than those of Sample I. However, SSD calculations reveal that their component subhalo orbital poles are actually more scattered on average than those of Sample I.

Following the evolution of Sample II planes back to $z = 1$, we see more substantial variations in plane thickness and larger average thickness values at virtually every timestep. Interestingly, the overlapping parameter spaces occupied by the paired and isolated halo configurations in Sample I break down somewhat for Sample II. Here, it is paired host haloes that have the largest plane thickness values at most timesteps – and by ∼20-50 kpc.

2.4.3 ELVIS: Sample III

As expected, the systematically larger plane dimensions of the Sample III population explain the increases observed in the full population (Sample II). In fact, because Sample III haloes are far more numerous than Sample I, the Sample II statistics almost exactly match those of Sample III.

Similarly, the co-rotation ratios of Sample III planes suggest slightly more

kinematic coherence than Sample I, thus accounting for the larger ratios seen in the combined Sample II. Interestingly, though, both Samples I and III have lower average SSDs, a fact which validates our sample selection methods and underscores the differences between the Sample I and III populations. The higher average SSD in the full sample, Sample II, clearly indicates that Samples I and III are more kinematically different than they are alike.

2.4.4 FIRE Latte results at $z = 0$

For the Latte sample in the DMO scenario (henceforth referred to as M12f-DMO and M12i-DMO), we find best-fit planes with RMS thicknesses of 12.9 kpc and 15.2 kpc, and corresponding RMS radii of 133.4 kpc and 98.1 kpc, respectively. These plane solutions are shown in Figure 2.11 and Figure 2.12 below.

As Figure 2.13 and Figure 2.14 demonstrate, neither Latte solution is particularly unique. While the M12i-DMO solution superficially appears more unique than that of M12f-DMO, it is worth noting that no solution for the former exceeds $\sim$37 kpc in thickness. Solutions for M12f-DMO, on the other hand, rarely exceed $\sim$50 kpc, though most are closer to $\sim$25 kpc.

By co-rotation ratio alone, both M12f-DMO and M12i-DMO seem to be minimally kinematically coherent. Only 9 out of the 15 subhaloes in the best-fit plane for M12f-DMO appear to be rotating in the same direction, while M12i-

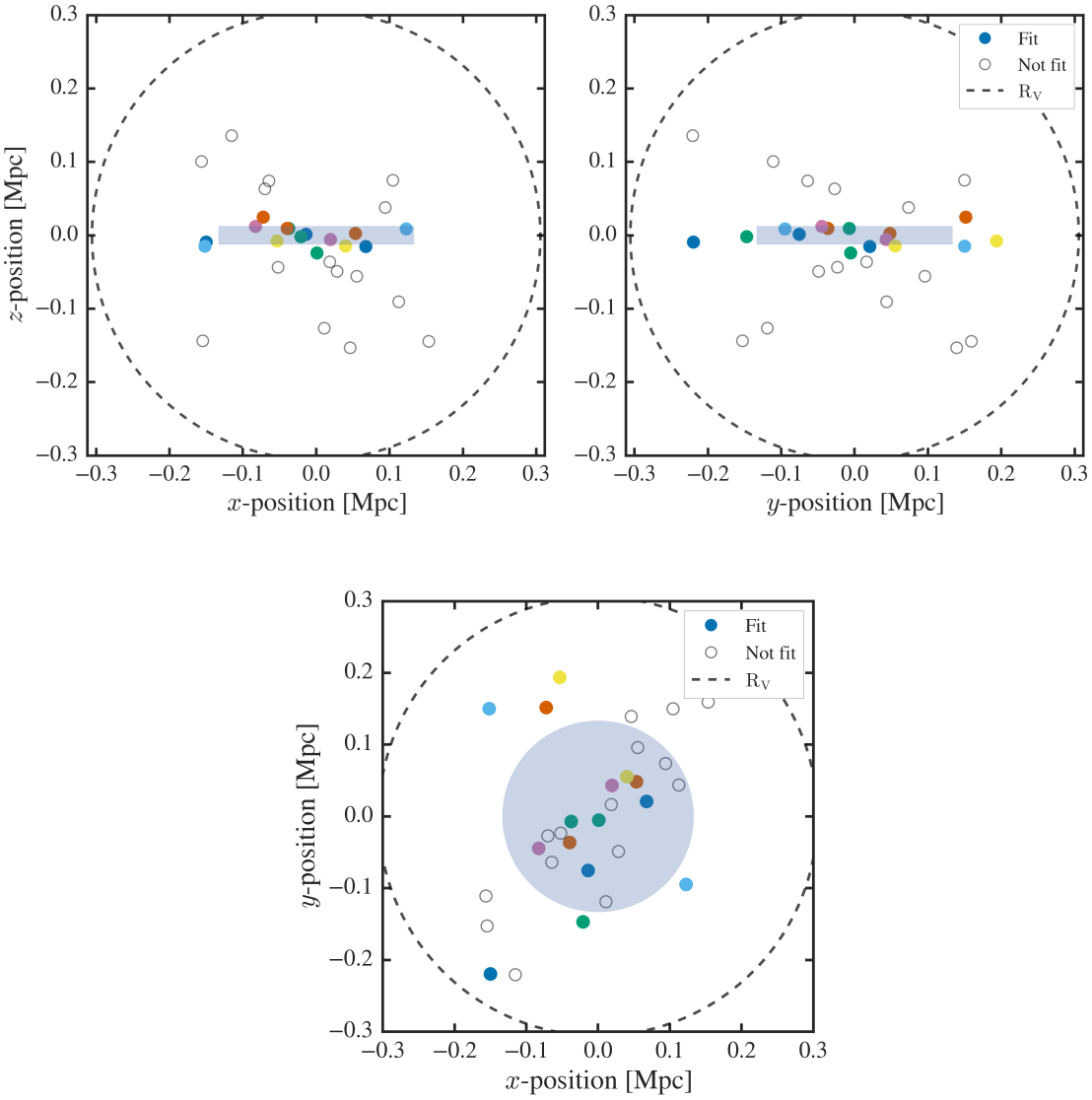

Figure 2.11: (*top*) Edge-on view and (*bottom*) face-on view of the $z = 0$ best-fit plane for the Latte halo M12f-DMO – with an RMS thickness and radius of 12.9 kpc and 133.4 kpc, respectively.

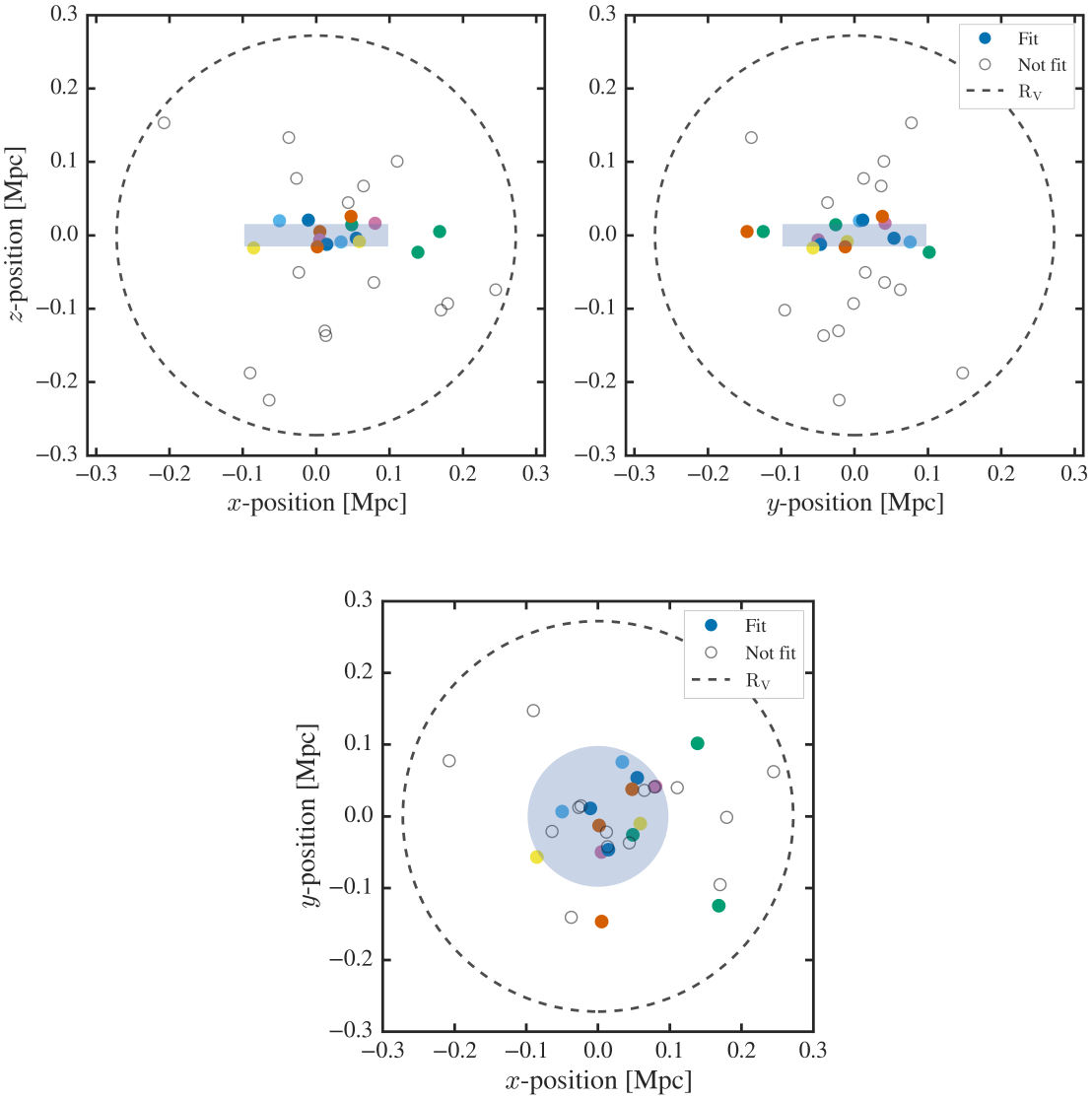

Figure 2.12: (*top*) Edge-on view and (*bottom*) face-on view of the $z = 0$ best-fit plane for the Latte halo M12i-DMO – with an RMS thickness and radius of 15.2 kpc and 98.1 kpc, respectively.

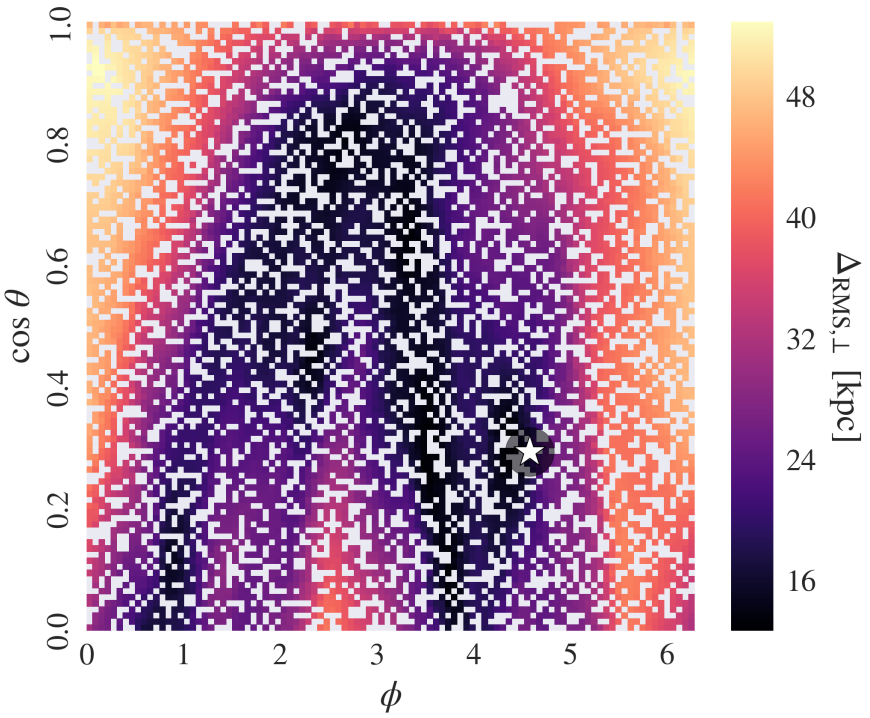

Figure 2.13: Uniqueness of the $z = 0$ best-fit plane for the Latte halo M12f-DMO. This plane solution is far from unique. In fact, no solution for the host exceeds an RMS thickness of $\sim$52 kpc.

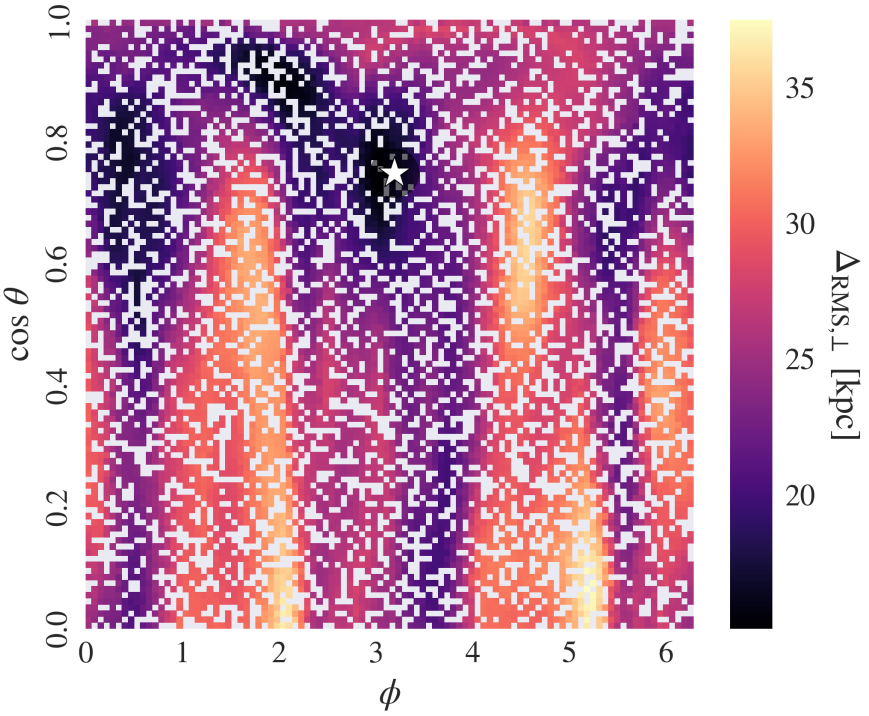

Figure 2.14: Uniqueness of the $z = 0$ best-fit plane for M12i-DMO. This plane solution is not particularly unique, and no solution for the host exceeds an RMS thickness of $\sim$37 kpc.

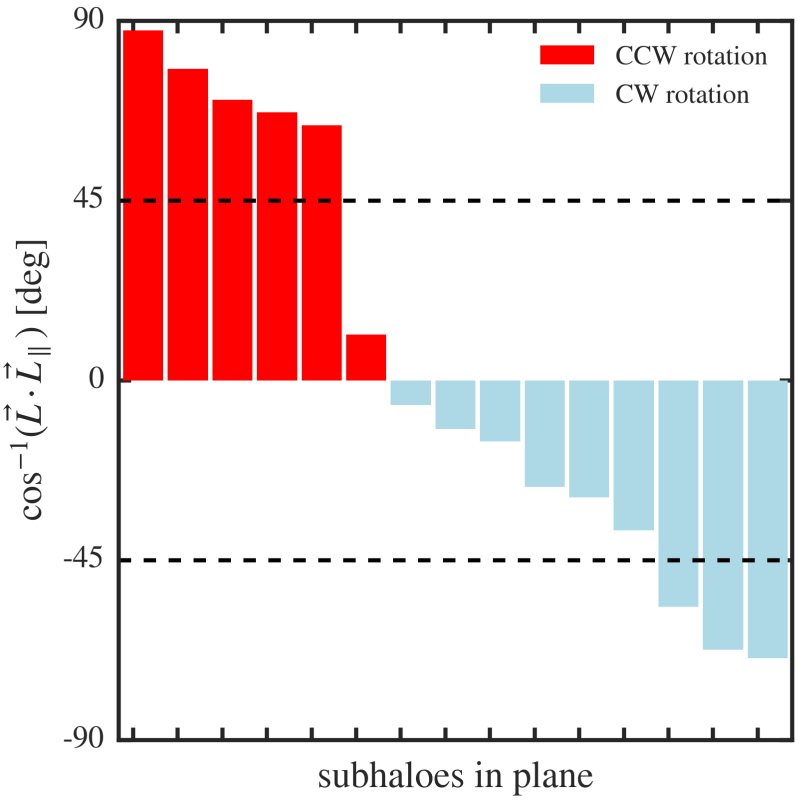

Figure 2.15: Kinematic breakdown of the $z = 0$ best-fit plane around Latte halo M12f-DMO. The dominant motion of the subhaloes is within the plane.

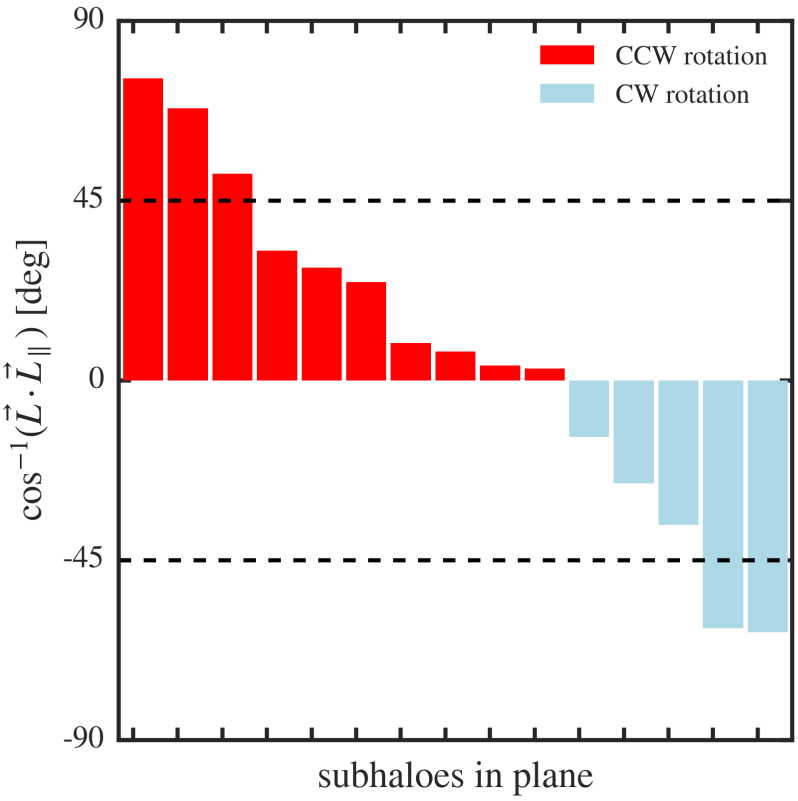

Figure 2.16: Kinematic breakdown of the $z = 0$ best-fit plane around Latte M12i-DMO. The dominant motion of the subhaloes is perpendicular to the plane.

DMO has 10 out of 15 subhaloes co-rotating. Breaking down these kinematics in Figure 2.15 and Figure 2.16, we see that in fact the dominant motion of M12i-DMO subhaloes is out of the plane. The motion of M12f-DMO subhaloes, on the other hand, is primarily within the plane, but just barely.

2.5 DM+disk Results

2.5.1 FIRE Latte results at $z = 0$

In the DM + stellar disk potential scenario, the Latte haloes (henceforth M12f-DM+d and M12i-DM+d) have slightly larger best-fit planes. We find RMS thicknesses of 18.4 kpc and 25.2 kpc, with corresponding RMS radii of 157.1 kpc and 166.6 kpc respectively (see Figure 2.17 and Figure 2.18) below.

Once again, examination of the thickness as a function of plane orientation (see Figure 2.19 and Figure 2.20) indicates that neither solution is particularly unique. More notable is the fact that the range of solution thicknesses increases for both haloes, with the M12i-DM+d plane getting as thick as $\sim$50 kpc and M12f-DM+d up to $\sim$75 kpc. This change, along with the increase in the thickness of the best-fit plane, could be explained by the contribution of the stellar disk potential, which is expected to destroy substructure at smaller radial distances (Garrison-Kimmel et al., 2017).

These halo solutions are also less strongly co-rotating, with ratios of 8 out

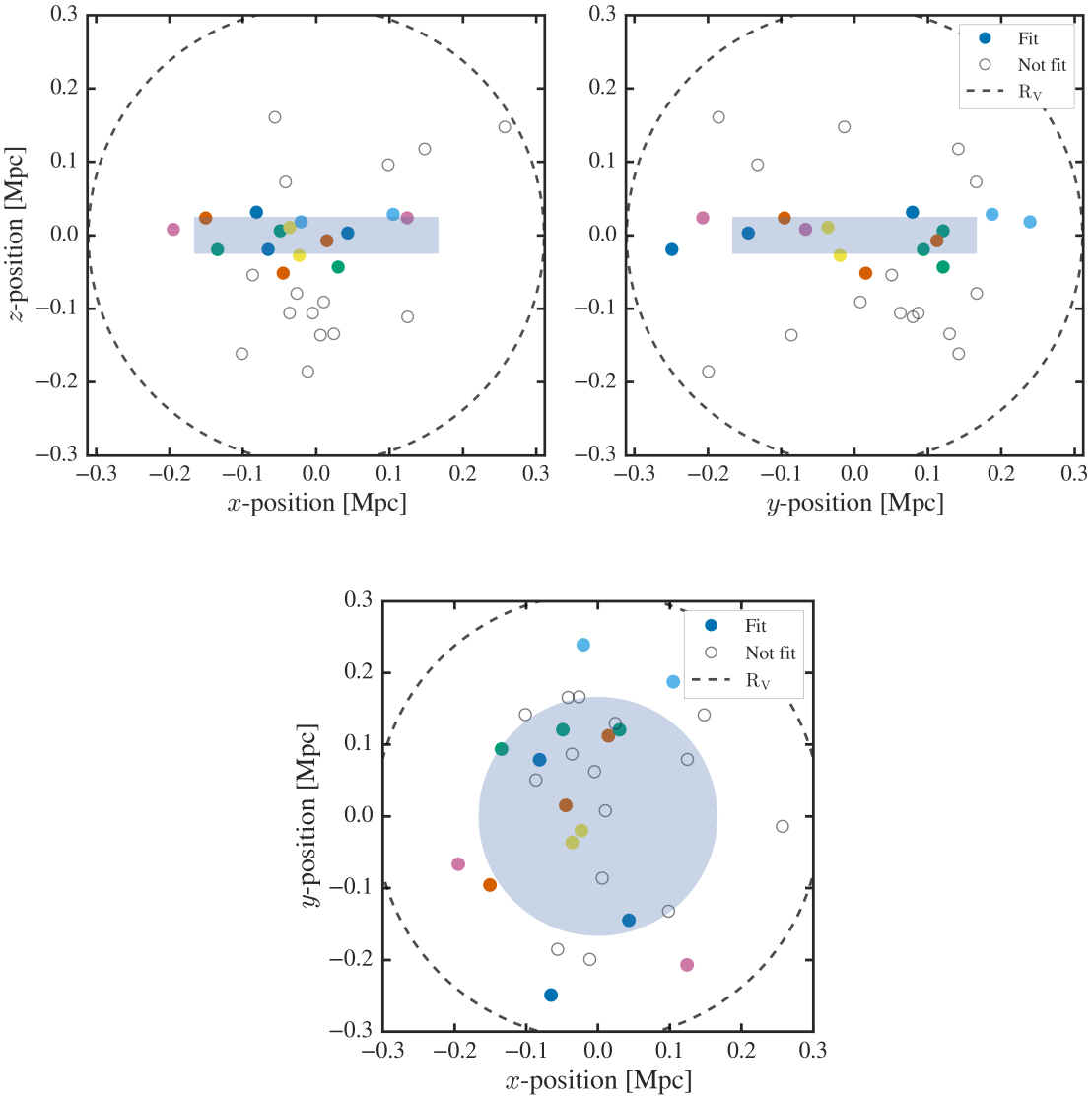

Figure 2.17: (*top*) Edge-on view and (*bottom*) face-on view of the $z = 0$ best-fit plane for the Latte halo M12f-DM+d – with an RMS thickness and radius of 25.2 kpc and 166.6 kpc, respectively.

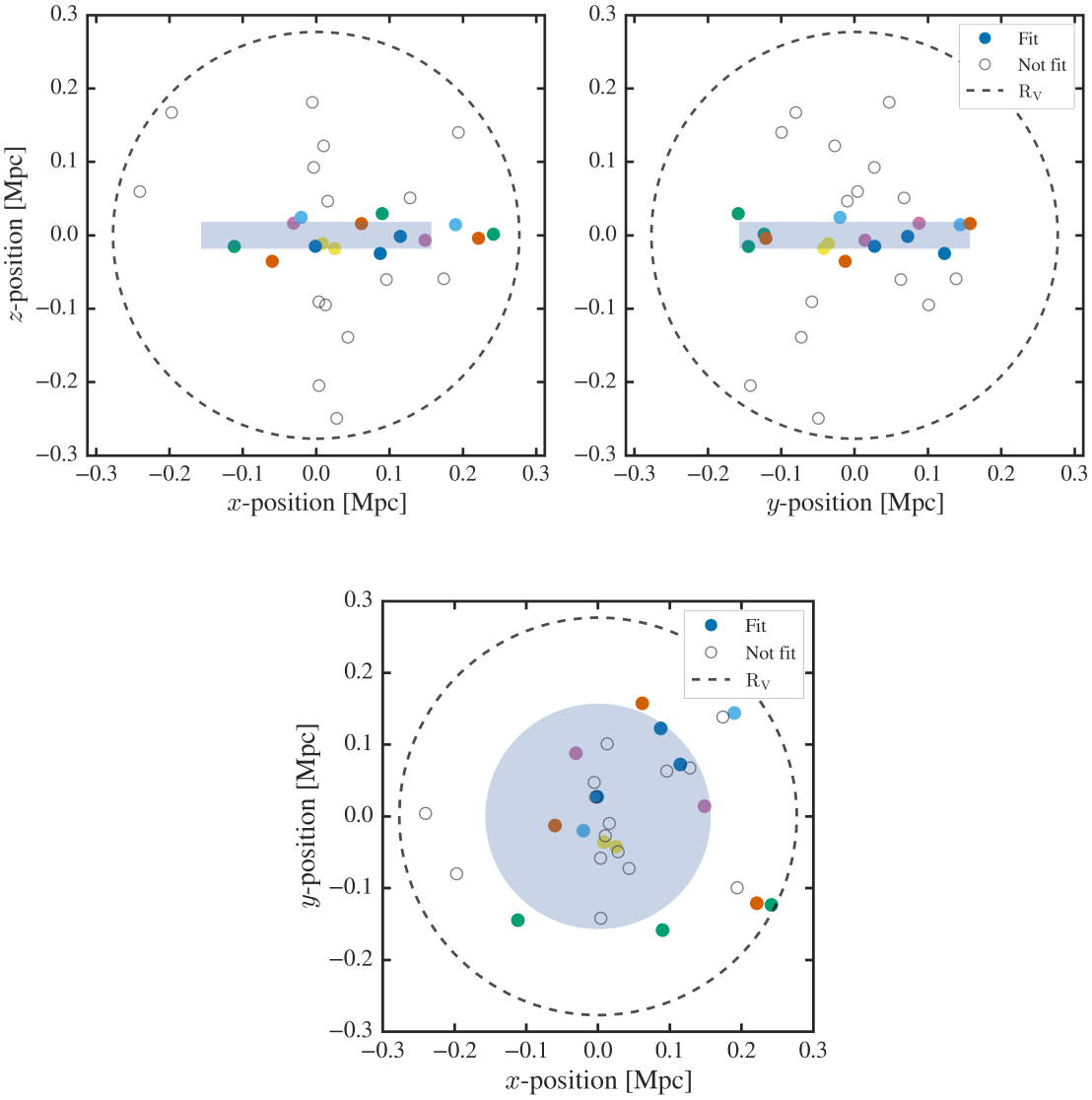

Figure 2.18: (*top*) Edge-on view and (*bottom*) face-on view of the $z = 0$ best-fit plane for the Latte halo M12i-DM+d – with an RMS thickness and radius of 18.4 kpc and 157.1 kpc, respectively.

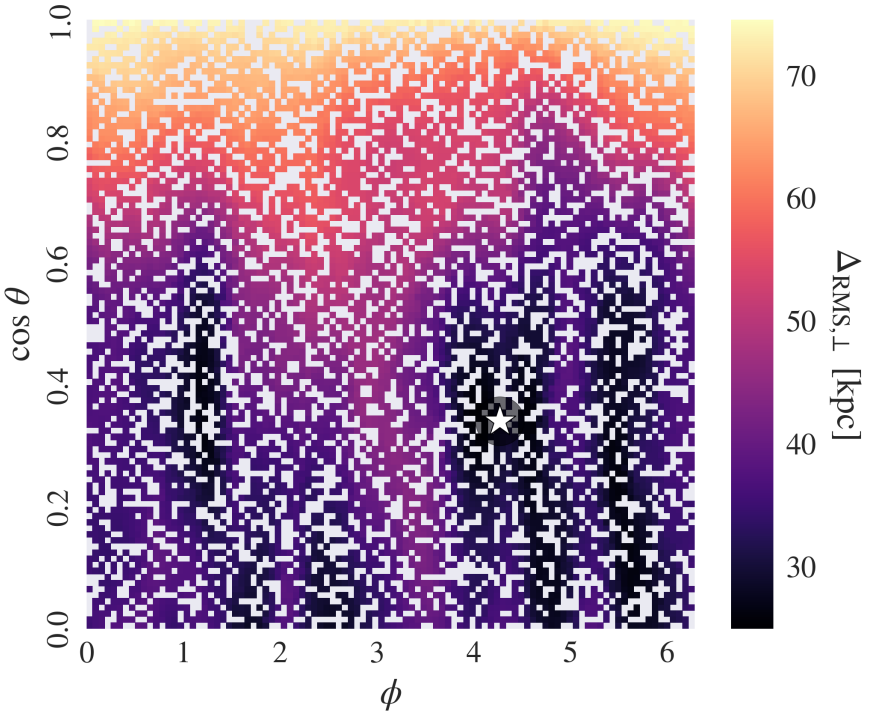

Figure 2.19: Uniqueness of the $z = 0$ best-fit plane for M12f-DM+d. This plane solution is far from unique, and no solution for the host exceeds an RMS thickness of $\sim$75 kpc.

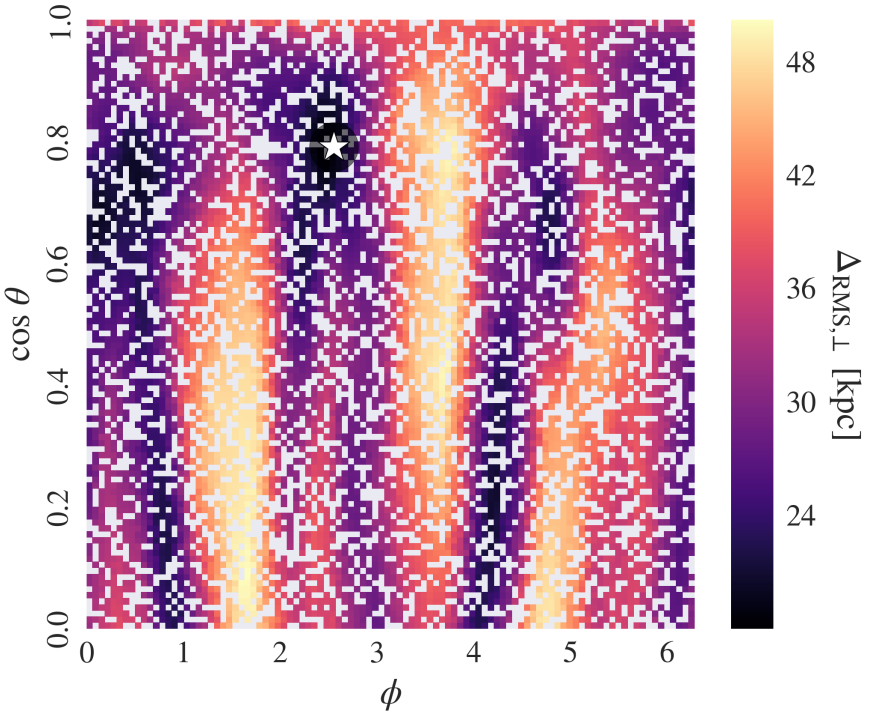

Figure 2.20: Uniqueness of the $z = 0$ best-fit plane for M12i-DM+d. This plane solution is not particularly unique, and no solution for the host exceeds an RMS thickness of $\sim$50 kpc.

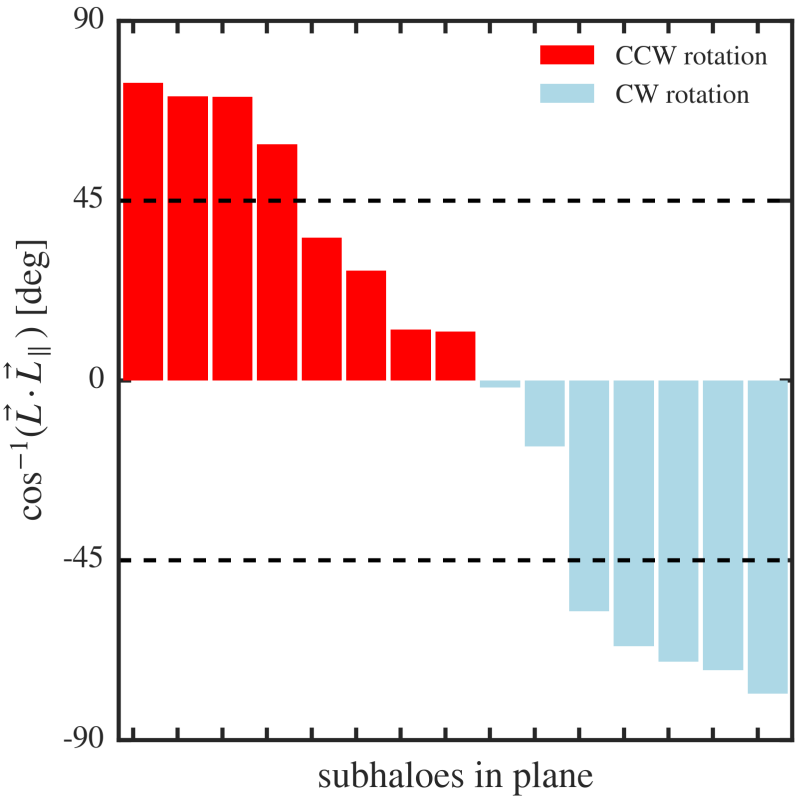

Figure 2.21: Kinematic breakdown of the $z = 0$ best-fit plane around Latte halo M12f-DM+d. The dominant motion of the subhaloes is within the plane.

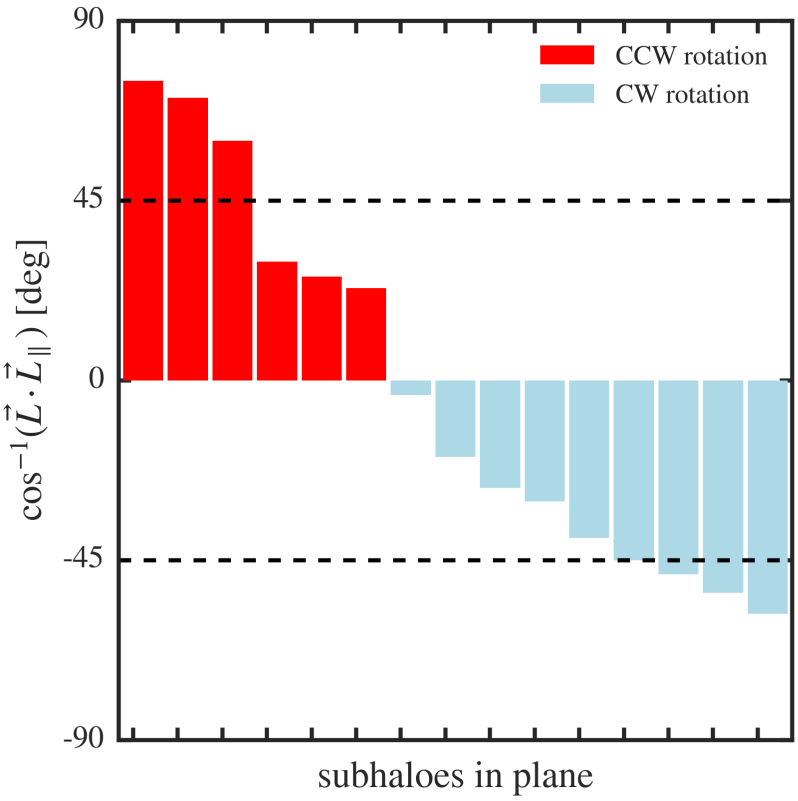

Figure 2.22: Kinematic breakdown of the $z = 0$ best-fit plane around Latte halo M12i-DM+d. The dominant motion of the subhaloes is perpendicular to the plane.

of 15 for M12f-DM+d and 9 out of 15 for M12i-DM+d. As shown Figure 2.21 and Figure 2.22 latter's motion is primarily out of the plane, while the former's is primarily within the plane by a small margin.

2.6 Discussion

By refining our "best-fit" plane definition for the initial ELVIS sample to 1) exclude subhaloes that lack gravitationally consistent progenitors and 2) focus on the population of subhaloes which orbit at least partially within the virial radius even at early times, we are able to find planes of satellites which are somewhat persistent over time and thus at least minimally kinematically coherent. However, their RMS thicknesses are, on average, nearly twice as large as those of observed planes described in the literature (for comparable radii).[2] As shown in Figure 2.10, the "highly statistically significant" M31 satellite plane described in Ibata et al. (2013) lies just at the edge of the parameter space occupied by our refined ELVIS sample. Thus, its dimensions alone are not implausible in this study. As illustrated in Figure 2.6, we are unable to recreate its co-rotation ratio (13 out of 15 plane satellite galaxies co-rotating[3]), although our larger kinematic analysis supports various

[2]Furthermore, many of these planes have an abundance of comparable thin-plane solutions at different orientations.

[3]But note that we are drawing our best-fit planes of 15 subhaloes from the 30 largest haloes (by peak virial mass) within the host's virial radius, compared to the 27 total satellites in Ibata et al. (2013)

criticisms regarding the utility of this metric (e.g., Buck et al., 2016).

Because our primary halo sample is drawn from a study designed in part to understand the relative importance of a large galactic companion in shaping local substructure, we first compare our plane subhalo properties to Garrison-Kimmel et al. (2014) results for the larger subhalo populations around paired vs. isolated hosts. The authors describe broad agreement between the formation times and concentrations of paired vs. isolated host haloes, as well as the abundance and kinematics of substructure within the virial radii of these hosts. The similarities break down in the region beyond the virial radius but within a distance of 1 Mpc (which they term the "Local Field"). In this region, paired environments have a much higher abundance of small haloes (even after subtracting subhaloes that lie within the companion's virial radius) and nearly twice as many subhaloes overall. Their kinematics are statistically "hotter and more complex," with whole subsets of subhaloes dominated by early interactions (Garrison-Kimmel et al., 2014).

Superficially, it would seem that only the region within a host halo's virial radius would be relevant to our study. Indeed, statistical properties of $z = 0$ planes are nearly identical between the paired and isolated host configurations. Following Sample I planes back to $z = 1$, these similarities arguably persist better than the plane properties themselves. However, Sample III (and, as a result, Sample II) properties begin to diverge. Paired hosts dominate the upper $\sim 20 - 50$ kpc of

the thickness parameter space from $0 < z < 1$, yet remain comparable to their isolated counterparts on the lower end. This seems to suggest some non-negligible contribution at earlier times from the more complex kinematics of the Local Field environment in paired host configurations.

The ELVIS haloes constitute our largest DMO sample, but they are not the whole story. As shown in Figure 2.10, the best-fit planes for our DMO Latte haloes are, at least by their axis ratios, outliers in this study. They are also quite varied in their properties for such a small sample, although their uniqueness and kinematics are unremarkable in the larger context of this study. Interestingly, the best-fit planes for our DM+disk Latte sample, more closely resemble our ELVIS DMO sample in Figure 2.10.

Comparing our best-fit planes for the FIRE Latte haloes in both the DMO and DM+disk scenarios to claims from the literature that the formation of statistically significant planes requires the destruction of satellites by a baryonic component (in particular, Ahmed et al., 2017), the results are inconclusive. It is certainly true that the depletion of substructure near the host halo is reflected in the increased dimensions of the planes in the DM+disk scenario. However, the small halo sample size – combined with the large scatter in plane properties – makes it difficult to draw any strong conclusions. We therefore consider claims from the literature about the importance of the baryonic contribution in creating statistically significant planes at

least *plausible* in this study – though Ahmed et al. (2017) use this logic to question the utility of DMO simulations in plane analyses, arguing that they are 'misleading.'

This argument is interesting in light of our finding that ELVIS DMO planes bear a stronger resemblance to the Latte DM+disk planes than their DMO counterparts – a comparison which turns out to be strengthened by our Sample I selection criteria. We look to detailed analyses of the Latte disk contribution for explanation and find the following: Garrison-Kimmel et al. (2017) state that, while the near-total destruction of the population of subhaloes that pass within ∼10-20 kpc of host galaxy seems to imply the preferential destruction of subhaloes "on radial, plunging orbits with low specific angular momentum," plots of the cumulative distribution of subhalo V_{tan} and V_{rad} values as a function of pericentric distance reveal that it is actually the tangential velocity distribution that is sensitive to the presence of the galactic disk. Subhaloes with lower tangential velocities will be significantly suppressed within $\sim$ 100 kpc of a given host when the disk contribution is included. Our ELVIS Sample I, selected to optimize the persistence of $z = 0$ planes across cosmic time, is dominated by long-term, highly-tangential orbits.[4] This brings our ELVIS DMO analysis closer to the Latte DM+disk results and to observational analyses like Cautun & Frenk (2017). In doing so, it seems to offer some remedy to the Garrison-Kimmel et al. (2017) finding that Latte DMO simulations over-predict

[4]This, as opposed to slowly infalling haloes with higher radial velocity components.

the number of subhaloes within ∼100 kpc with $V_{tan} < 100$ km s^{-1} by a factor of ten – as well as criticisms of plane studies using DMO simulations (Ahmed et al., 2017).

2.7 Conclusion

In this work, we use Local Group analog haloes from the ELVIS and FIRE Latte simulations to assess observational claims regarding planes of satellite galaxies around the Milky Way and Andromeda. We present a refined ELVIS subhalo sample designed to maximize plane persistence over time, and find that its $z = 0$ plane properties are not entirely inconsistent with observational claims, though their bulk statistics suggest thicker planes with less coherent kinematics. The effects of our ELVIS sample selection criteria compare quite favorably to findings from Garrison-Kimmel et al. (2017) that a stellar disk potential preferentially destroys subhaloes with low tangential velocities, and we therefore conclude that thoughtful sample selection could ameliorate similar DMO studies.

Though results for even our most optimistic DMO sample seem to support earlier claims that observed planes in the literature are merely chance alignments of satellites with misleading line-of-sight kinematics, we acknowledge that we cannot fully recreate the robust properties touted in some systems and leave it to future studies to determine if these differences can be explained by such factors as the

plane orientation relative to the host's galactic disk (or to the vector connecting the host galaxy and a massive companion), the viewing angle of the system, etc.

Bibliography

Ahmed S. H., Brooks A. M., Christensen C. R., 2017, MNRAS, 466, 3119

Behroozi P. S., Wechsler R. H., Wu H.-Y., 2013a, ApJ, 762, 109

Behroozi P. S., Wechsler R. H., Wu H.-Y., Busha M. T., Klypin A. A., Primack J. R., 2013b, ApJ, 763, 18

Bellazzini M., Oosterloo T., Fraternali F., Beccari G., 2013, A&A, 559, L11

Buck T., Macciò A. V., Dutton A. A., 2015, ApJ, 809, 49

Buck T., Dutton A. A., Macciò A. V., 2016, MNRAS, 460, 4348

Bullock J. S., Boylan-Kolchin M., 2017, ARA&A, 55, 343

Cautun M., Frenk C. S., 2017, MNRAS, 468, L41

Cautun M., Bose S., Frenk C. S., Guo Q., Han J., Hellwing W. A., Sawala T., Wang W., 2015, MNRAS, 452, 3838

Chiboucas K., Karachentsev I. D., Tully R. B., 2009, AJ, 137, 3009

D'Onghia E., Springel V., Hernquist L., Keres D., 2010, ApJ, 709, 1138

Garrison-Kimmel S., Boylan-Kolchin M., Bullock J. S., Lee K., 2014, MNRAS, 438, 2578

Garrison-Kimmel S., et al., 2017, MNRAS, 471, 1709

Ibata R. A., et al., 2013, Nature, 493, 62

Kirby E. N., Cohen J. G., Guhathakurta P., Cheng L., Bullock J. S., Gallazzi A., 2013, ApJ, 779, 102

Knollmann S. R., Knebe A., 2009, ApJS, 182, 608

Koch A., Grebel E. K., 2006, AJ, 131, 1405

Kroupa P., 2012, Publ. Astron. Soc. Australia, 29, 395

Libeskind N. I., Frenk C. S., Cole S., Helly J. C., Jenkins A., Navarro J. F., Power C., 2005, MNRAS, 363, 146

Lynden-Bell D., 1976, MNRAS, 174, 695

Metz M., Kroupa P., Libeskind N. I., 2008, ApJ, 680, 287

Müller O., Jerjen H., Pawlowski M. S., Binggeli B., 2016, A&A, 595, A119

Müller O., Pawlowski M. S., Jerjen H., Lelli F., 2018, Science, 359, 534

Müller O., Rejkuba M., Pawlowski M. S., Ibata R., Lelli F., Hilker M., Jerjen H., 2019, A&A, 629, A18

Pawlowski M. S., McGaugh S. S., 2014, ApJ, 789, L24

Pawlowski M. S., Kroupa P., Angus G., de Boer K. S., Famaey B., Hensler G., 2012, MNRAS, 424, 80

Pawlowski M. S., Kroupa P., Jerjen H., 2013, MNRAS, 435, 1928

Pawlowski M. S., McGaugh S. S., Jerjen H., 2015, MNRAS, 453, 1047

Recchi S., Kroupa P., Ploeckinger S., 2015, MNRAS, 450, 2367

Tully R. B., Libeskind N. I., Karachentsev I. D., Karachentseva V. E., Rizzi L., Shaya E. J., 2015, ApJ, 802, L25

Wetzel A. R., Hopkins P. F., Kim J.-h., Faucher-Giguère C.-A., Kereš D., Quataert E., 2016, ApJ, 827, L23